Materials Transactions, Vol. 54, No. 8 (2013) pp. 1535 to 1538

RAPID PUBLICATION

Magnetoelastic Anomalies Exhibited by Ni–Fe(Co)–Ga Polycrystalline Ferromagnetic Shape Memory Alloy

Patricia Lázpita[1], Volodymyr A. Chernenko[1,2], Jose M. Barandiarán[1], Jon Gutiérrez[1], Hideki Hosoda[3] and Jose A. Rodríguez-Velamazán[4,5]

[1]*BCMaterials and Universidad del País Vasco, UPV/EHU, P. O. Box 644, Bilbao 48080, Spain*
[2]*Ikerbasque, Basque Foundation for Science, Bilbao 48011, Spain*
[3]*Tokyo Institute of Technology, Yokohama 226-8503, Japan*
[4]*Instituto de Ciencia de Materiales de Aragón, CSIC-Universidad de Zaragoza, Zaragoza 50009, Spain*
[5]*Institute Laue-Langevin, Grenoble Cedex 38042, France*

The martensitic transformation (MT) as well as the structure, magnetic and magnetostrain properties of a polycrystalline $Ni_{50.1}Fe_{18.6}Ga_{27.2}Co_{4.1}$ (at%) ferromagnetic shape memory alloy are investigated. The studied alloy exhibits a martensitic ferromagnetic phase near room temperature that shows a non-modulated tetragonal structure with a tetragonality ratio of $c/a > 1$. Strain measurements reveal a complex spontaneous change at MT amounting to about 0.15% that increases up to 0.22% at 5 T of the applied magnetic field indicating orientation influence of the field on the martensitic variants growth. Magnetostrain measurements enable evaluation of the magnetic field-induced strain effect in the vicinity of MT. The sample shows moderate deformation achieving values of 70 ppm related to the magnetization rotation and volume magnetostriction that does not saturate at applied magnetic field of 5 T. [doi:10.2320/matertrans.M2013154]

(Received April 22, 2013; Accepted June 3, 2013; Published July 25, 2013)

Keywords: *ferromagnetic shape memory alloys, magnetoelasticity, nickel–iron(cobalt)–gallium*

1. Introduction

Ferromagnetic shape memory alloys have been drawing a lot of interest during the last years due to the possibility to obtain magnetically induced strains up to 10%[1)] opening a new class of magnetically controlled actuator materials. The coupling of the structural and magnetic degrees of freedom triggers a rearrangement of the crystallographic domains under applied magnetic field giving rise to the magnetic field induced strain (MFIS) effect. The enhanced fragility of the prototype Ni–Mn–Ga[2,3)] Heusler alloys led to the extensive efforts in the research of new materials like Fe–Pt,[4)] Fe–Pd,[5)] Co–Ni–Ga,[6)] Co–Ni–Al[7)] and Ni–Mn–(In, Sn, Sb).[8–10)]

Among alternative compounds, the Ni–Fe–Ga alloys are considered to be promising materials due to improved mechanical properties. These compounds exhibit MFIS and a large superelastic strain in a wide temperature window. The Curie temperature of these materials is close to room temperature so they present a reduced magnetocrystalline anisotropy constant at this temperature that prevents a MFIS effect to be as large as in the Ni–Mn–Ga alloys. The increase in the Curie temperature and maintaining the martensitic transformation (MT) temperature around room temperature are necessary for further developing of this effect. It has been shown in a number of publications that Co addition is an efficient way to fulfill this task.[11–13)]

Similarly to the other FSMAs, the structure, mechanical and magnetic properties of the martensitic phase of Ni–Fe–Ga alloys strongly depend on the composition and adding of fourth element. Different studies have been carried out in order to determine these properties and to evaluate the MFIS effect in Ni–Fe–Ga doped by Co. The majority of publications are related to a single crystalline state of these alloys. Particularly, a giant MFIS of 8.5% at room temperature under static mechanical stress was achieved for $Ni_{49}Fe_{18}Ga_{27}Co_6$ (at%) alloy.[11,14,15)] On the other hand, less works have been done in order to clarify the MFIS effect in the bulk polycrystalline materials as they are of high interest due to their less complex manufacturing.

The aim of this study is the characterization of the structural and magnetic properties of as-quenched bulk polycrystalline $Ni_{50.1}Fe_{18.6}Ga_{27.2}Co_{4.1}$ (at%) alloy. We also try to determine the feasibility to develop the MFIS effect in this compound studying the magnetostrain behavior.

2. Experimental Procedure

The ingot was prepared by induction melting of high purity iron, nickel, gallium and cobalt, with a subsequent casting into a copper mold. The ingot was sealed in a quartz capsule filled with argon gas, heat treated at 1173 K during 72 h and quenched into water. The chemical composition of $Ni_{50.1}Fe_{18.6}Ga_{27.2}Co_{4.1}$ (at%) was determined by the energy-dispersive X-ray spectroscopy. The sample surface was mechanically polished and electropolished to examine its microstructure by optical microscopy. During electro-polishing, the electrolyte composed of nitric acid (33 vol%) and methanol (67 vol%) was kept at 230 K and a voltage in the range of 10–15 V was applied to the sample.

Neutron thermodiffraction experiments were carried out in the D1B instrument of the Institute Laue Langevin (Grenoble) to determine an evolution of the structure across the MT. The diffraction patterns were obtained in a range of temperatures between 150 and 340 K using a wavelength of 0.252 nm. In order to reduce an influence of texture, the sample was rotating during the experiments.

The MT was characterized by Differential Scanning Calorimetry (DSC). Magnetization measurements were carried out with a vibrating sample magnetometer (VSM).

Strain was measured for two different configurations by gluing the strain gauge perpendicular and parallel to the columnar grain structure determined by optical microscopy.

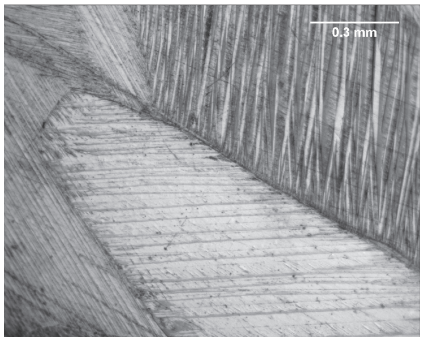

Fig. 1 The grain structure and martensitic morphology of Ni–Fe(Co)–Ga alloy. The black spots inside of the grains and their colonies on the grain boundaries represent precipitates of gamma-phase (see text for details).

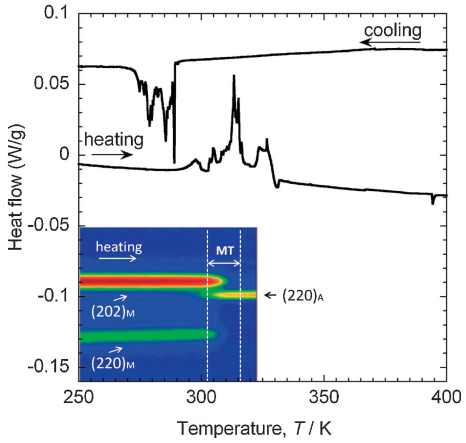

Fig. 2 DSC curves and neutron thermodiffraction patterns (inset) evidencing the martensitic transformation in the studied alloy. The temperature dependences of intensities of reflections in the inset clearly show the occurrence of martensitic transformation.

Magnetostrain measurements were done in fields up to 5 T and temperature range between 200 and 320 K. These measurements were done in a platform from Cryogenic Ltd. using a Wheatstone bridge with a noise level of 0.2×10^{-6}.

3. Results and Discussion

The optical microscopy image (Fig. 1) presents a columnar structure showing large grains of 300–600 μm in thickness and 1–3 mm in length. At room temperature, the grains consist of differently oriented twin variants related to the martensitic microstructure indicating that the MT temperature in this alloy is above room temperature. The existence of a heterogeneous distribution of grain size involves the presence of internal stresses which can promote a local micro-cracks initiation.[16] Furthermore, the small particles of the gamma-phase inside of the grains and their colonies on the grain boundaries are observed in Fig. 1. The presence of gamma-phase (fcc solid solution enriched by Fe) is well-known phenomenon for the Ni–Fe–Ga alloys. Even though an occurrence of these precipitates inside of the grains reduces the brittleness of the sample, the cracks may start to propagate after thermal cycling across MT and the specimen may collapse by intergranular fractures promoted the precipitates on the grain boundaries. These behaviors have been already described for Ni–Fe–Ga polycrystalline alloys.[17]

The calorimetric curves were obtained in the heating and cooling runs (see Fig. 2). The MT proceeds in an extended range of temperatures both in the reverse and direct process as usually in the as-quenched alloys.[18] Several DSC maximums, not clearly separated in different stages, are observed between 294 and 330 K during heating. This behavior is related to the elastic energy stored during the first steps of the transformation that induce the appearance of the subsequent steps as proposed by Seguí *et al.*[19] Whereas the DSC measurements show MT in the extended range of temperatures, the neutron diffraction patterns collected during the heating show this MT in a narrower range between 301 and 317 K (inset to Fig. 2). The non-coincident results obtained with these techniques could be attributed to the concentration variation of the alloy since different pieces of the same ingot were used to do the different experiments.

Figure 3(a) shows the neutron diffraction patterns collected during heating. The peaks at different temperatures were indexed in terms of a $L2_1$-ordered cubic lattice with cell

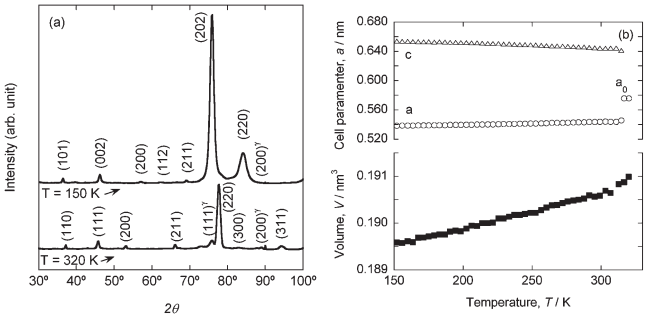

Fig. 3 (a) Experimental neutron diffraction patterns in the martensitic and austenitic phase collected during heating. The precipitates of γ-phase are indicated as well. (b) Temperature dependences of the unit cell parameters and cell volume during heating.

parameter $a_0 = 0.575$ nm at 320 K in the austenite phase and a tetragonal non-modulated structure in the martensitic phase at 150 K with cell parameters of $a = 0.5383$ nm and $c = 0.6544$ nm ($c/a = 1.22$) related to the cubic coordinate system. Figure 3(b) depicts the evolution of the cell parameters during heating. The transformation volume change estimated from the cell volume dependence in the bottom panel in Fig. 3(b) is equal to about 0.1%. Notably, the sample presents a small amount of disordered fcc gamma-phase[20,21] consistent with the precipitates observed in the optical microscopy image. The reflections of the gamma-phase shown in Fig. 3(a) provide its unit cell parameter of 0.359 nm. The diffraction pattern indicates a high degree of 220 texture in the austenitic phase. Based on Fig. 3(b), the linear expansion coefficient of the martensitic phase was evaluated to be equal to 12.8×10^{-6}/K in the temperature range from 200 to 300 K. This value is in line with the coefficients of linear thermal expansion for Ni (13.3×10^{-6}/K) and Fe (12.1×10^{-6}/K).

Figure 4 depicts temperature dependences of the strain in the vicinity of MT measured perpendicular and along the columnar microstructure of the material using two different pieces of alloy. The perpendicular strain (Fig. 4(a)) exhibits a complex and sharp change at MT amounting to about 0.15%. It has to be noted that the negative slope in the martensitic and austenitic phases is due to an uncorrected instrumental

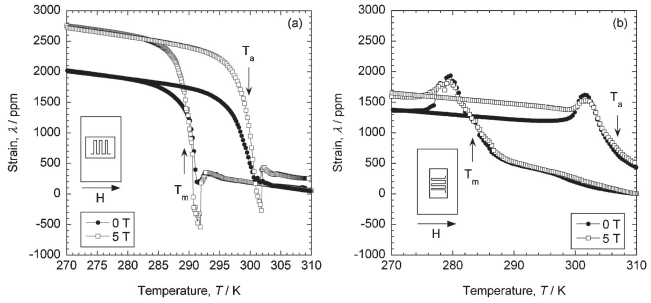

Fig. 4 (a) Strain versus temperature measured perpendicular to the columnar structure under 0 and 5 T. (b) Strain versus temperature measured parallel to the columnar structure under 0 and 5 T. In both cases the magnetic field was applied in the direction perpendicular to the columnar structure. The transformation temperatures are indicated by arrows.

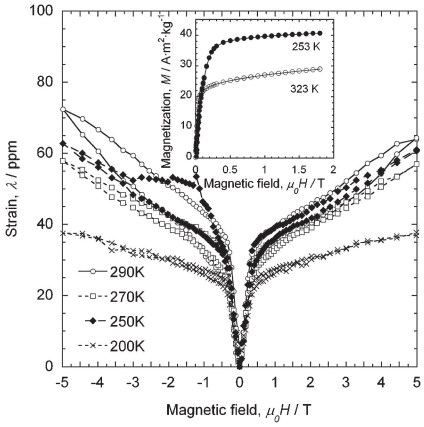

Fig. 5 Deformation as a function of temperature measured perpendicular to the columnar structure with the magnetic field applied along a gauge. The inset shows the magnetization curves for the austenitic and martensitic phases, respectively.

drift produced by the thermal expansion difference between the specimens and the strain gauges. The temperature dependence of the strain in the martensitic and austenitic phases was neglected because the focus in the present work has been made on the transformation region only.

At cooling across the forward MT characterized by temperature T_m, the sample starts to contract in the direction of measurement followed by its strong expansion. In the reverse transformation at T_a, the sample recovers deformation in the reverse manner. The jump-like strain behavior during MT is a typical feature occurring in both the ordinary nonmagnetic shape memory alloys and FSMAs. However, in the most studied FSMAs, the alloys with $c/a < 1$ show a contraction as the main part of the strain change during the forward MT, followed by an expansion in the reverse one. The present work supports the point of view proposed Chen *et al.*[22] that the difference in strain behavior is related to the parameter c/a. According to this point of view, the alloys with $c/a < 1$ suffer a spontaneous contraction[23,24] while those with $c/a > 1$ present an expansion[22,25] during the transformation from the parent phase to the martensitic one which is the case of the studied sample in the present work. Just described correlation between strain behavior and c/a ratio could be considered as an empirical fact which is still needed to be confirmed and understood by further more focused studies.

An application of magnetic field does not produce a significant shift of the martensitic transformation temperatures (Fig. 4(a)). Instead, the field-assisted growth of preferably orientated variants with the easy axes along the applied magnetic field is observed in the form of initial sharp decrease of strain resulting in an increase of the total strain change to about of 0.22%. This behavior reflects a competition between this preferential orientation and the spontaneous self-accommodation of martensite in each grain in the polycrystalline textured sample.

When the spontaneous strain is measured along the columnar structure (Fig. 4(b)), the forward transformation is accompanied by the initial expansion followed by contraction behavior, this sequence being reciprocal to the perpendicular case as expected from the conservation volume principle. The incomplete recovery in this case is attributed to a residual strain related to some amount of martensite remaining after the thermal cycling.[26,27]

As already mentioned, for the first configuration it is notably that at MT start there appears an initial decrease of the strain that recovers when transformation is in progress. On the other hand, the deformation parallel to the microstructure presents a maximum. The sample suffers an initial expansion followed by a contraction. As the other possible explanation, these anomalies can be related to the elastic modulus softening in the presence of the local compressive/tensile internal stresses induced by MT in an anisotropic polycrystal.[28]

Figure 5 shows magnetostriction curves measured perpendicular to the columnar microstructure when the applied magnetic field, up to 5 T, is parallel to the columnar microstructure at different temperatures during step-wise cooling. The magnetostriction curves show hysteresis and values between 25 and 40 ppm at low applied magnetic field of about 0.5 T. For higher applied magnetic field, the strain continues increasing without saturation which is also correlated with the behavior of magnetization remaining still nonsaturated at high magnetic field (inset to Fig. 5). A fast growth of the strain at low magnetic field is related to the magnetization rotation as indicates the quadratic dependence of the magnetostriction versus magnetization (Fig. 6). The volume magnetostriction effect can explain the linear dependence at higher magnetic fields seen in Fig. 5. The magnetostriction achieves the maximum value in the vicinity of the martensitic transformation temperature similarly as was already observed in other FSMAs and attributed to the softening of the elastic constants at temperatures around MT.[29–31]

The magnetostrain parallel to the columnar microstructure was also measured revealing a value of -10 ppm at temperatures around 300 K for an applied magnetic field of 5 T parallel to the columnar structure (not shown).

The aforementioned anisotropic magnetostrain behavior is in line with the previously observed trends indicating influence of elongated grain structure on the magnetostrain response.[18]

Although the sample exhibits texture that could improve a preferential orientation of the martensitic variants getting better strain properties under applied magnetic field or

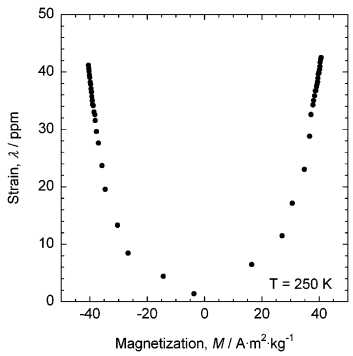

Fig. 6 Magnetostriction dependence as a function of the magnetization measured up to 1.8 T in the martensitic state. This dependence shows a quadratic behavior of the strain with respect to the magnetization indicating a magnetization rotation as a mechanism of the magnetostriction.

mechanical stress, this texture and large grains were not enough conditioned to observe a large magnetostrain effect (MSE). Note, that the magnetic field-induced strain in this Ni–Fe(Co)–Ga sample is about 70 ppm at room temperature for applied magnetic field of 5 T, which is similar in the magnitude achieved in many cases of the bulk Ni–Mn–Ga polycrystalline alloys.[18,29] In order to achieve a large MSE, some thermomechanical training procedure must be applied to reduce a twinning stress. The stress–strain cycling in our case was hindered by the brittleness of samples. This is, probably, because the grain size was not optimized and because the rapid quenching did not produce enough volume fraction of gamma-particles to improve the alloy ductility.

4. Conclusions

The $Ni_{50.1}Fe_{18.6}Ga_{27.2}Co_{4.1}$ ferromagnetic shape memory alloy was fabricated. It shows a 220 grain texture and exhibits a tetragonal martensitic phase with $c/a > 1$ at room temperature. The martensitic transformation is accompanied by the specific volume change of 0.1%. The sample exhibits a spontaneous change in the strain of about 0.15% during the martensitic transformation that increases until 0.22% when magnetic field of 5 T is applied. The magnetostrain measurements show moderate strains achieving values of 70 ppm that do not saturate at applied magnetic field of 5 T. The magnetostrain behavior is interpreted as related to the magnetization rotation and volume magnetostriction. A small amount of gamma-phase did not improve essentially the ductility of alloy whereby preventing its mechanical training to decrease twinning stress. In the further work, the grain size and heat treatment of the alloy must be optimized in order to allow its thermomechanical training and obtaining large MSE.

Acknowledgments

This work has been carried out with the financial support of the Project No. MAT2011-28217 C02-02, by the Spanish Ministry of Science and Innovation. Technical and human support provided by SGIker is gratefully acknowledged. One of authors (H.H.) appreciates a financial support (NEXT program LR015, 2010–2013) from the Japan Society for the Promotion of Science (JSPS).

REFERENCES

1) A. Sozinov, A. A. Likhachev, N. Lanska and K. Ullakko: Appl. Phys. Lett. **80** (2002) 1746–1748.
2) V. V. Martynov: J. Phys. IV **05** (1995) C8-91–C8-99.
3) K. Ullakko, J. K. Huang, C. Kantner, R. C. O'Handley and V. V. Kokorin: Appl. Phys. Lett. **69** (1996) 1966–1968.
4) T. Kakeshita, T. Takeuchi, T. Fukuda, M. Tsujiguchi, T. Saburi, R. Oshima and S. Muto: Appl. Phys. Lett. **77** (2000) 1502–1504.
5) J. Cui and R. D. James: IEEE Trans. Magn. **37** (2001) 2675–2677.
6) M. Wuttig, J. Li and C. Craciunescu: Scr. Mater. **44** (2001) 2393–2397.
7) K. Oikawa, L. Wulff, T. Iijima, F. Gejima, T. Ohmori, A. Fujita, K. Fukamichi, R. Kainuma and K. Ishida: Appl. Phys. Lett. **79** (2001) 3290–3292.
8) R. Kainuma, Y. Imano, W. Ito, H. Morito, Y. Sutou, K. Oikawa, A. Fujita, K. Ishida, S. Okamoto, O. Kitakami and T. Kanomata: Appl. Phys. Lett. **88** (2006) 192513.
9) K. Oikawa, W. Ito, Y. Imano, Y. Sutou, R. Kainuma, K. Ishida, S. Okamoto, O. Kitakami and T. Kanomata: Appl. Phys. Lett. **88** (2006) 122507.
10) Y. Sutou, Y. Imano, N. Koeda, T. Omori, R. Kainuma, K. Ishida and K. Oikawa: Appl. Phys. Lett. **85** (2004) 4358–4360.
11) H. Morito, K. Oikawa, A. Fujita, K. Fukamichi, R. Kainuma, K. Ishida and T. Takagi: J. Magn. Magn. Mater. **290–291** (2005) 850–853.
12) K. Oikawa, Y. Imano, V. A. Chernenko, F. Luo, T. Omori, Y. Sutou, R. Kainuma, T. Kanomata and K. Ishida: Mater. Trans. **46** (2005) 734–737.
13) H. X. Zheng, J. Liu, M. X. Xia and J. G. Li: J. Alloy. Compd. **387** (2005) 265–268.
14) H. Morito, A. Fujita, K. Oikawa, K. Ishida, K. Fukamichi and R. Kainuma: Appl. Phys. Lett. **90** (2007) 062505.
15) H. Morito, K. Oikawa, A. Fujita, K. Fukamichi, R. Kainuma and K. Ishida: Scr. Mater. **53** (2005) 1237–1240.
16) A. Boumaiza, N. Rouag, T. Baudin, Z. Larouk and R. Penelle: J. Phys.: Conf. Ser. **240** (2010) 012036.
17) F. Masdeu, J. Pons, R. Santamarta, E. Cesari and J. Dutkiewicz: Mater. Sci. Eng. A **481–482** (2008) 101–104.
18) M. Pasquale, C. Sasso, S. Besseghini, F. Passaretti, E. Villa and A. Sciacca: IEEE Trans. Magn. **36** (2000) 3263–3265.
19) C. Seguí, V. A. Chernenko, J. Pons and E. Cesari: J. Phys. IV France **112** (2003) 903–906.
20) J. Sui, Z. Gao, H. Yu, Z. Zhang and W. Cai: Scr. Mater. **59** (2008) 874–877.
21) Y. Imano, T. Omori, K. Oikawa, Y. Sutou, R. Kainuma and K. Ishida: Mater. Sci. Eng. A **438–440** (2006) 970–973.
22) F. Chen, X. L. Meng, W. Cai, L. C. Zhao and G. H. Wu: J. Magn. Magn. Mater. **302** (2006) 459–462.
23) Y. Li, C. Jiang, T. Liang, Y. Ma and H. Xu: Scr. Mater. **48** (2003) 1255–1258.
24) V. A. Chernenko, J. M. Barandiarán, V. A. L'vov, J. Gutiérrez, P. Lázpita and I. Orue: J. Alloy. Compd. (2012) doi:10.1016/j.jallcom.2011.12.117.
25) K. Oikawa, R. Saito, K. Anzai, H. Ishikawa, Y. Sutou, T. Omori, A. Yoshikawa, V. A. Chernenko, S. Besseghini, A. Gambardella, R. Kainuma and K. Ishida: Mater. Trans. **50** (2009) 934–937.
26) C. Seguí, V. A. Chernenko, J. Pons, E. Cesari, V. Khovailo and T. Takagi: Acta Mater. **53** (2005) 111–120.
27) R. Santamarta, E. Cesari, J. Pons and T. Goryczka: Metall. Mater. Trans. A **35** (2004) 761–770.
28) R. Santamarta, J. Pons and E. Cesari: J. Phys. IV **11** (2001) Pr8-351–Pr8-356.
29) J. M. Barandiarán, V. A. Chernenko, J. Gutiérrez, I. Orúe and P. Lázpita: Appl. Phys. Lett. **100** (2012) 262410.
30) L. Mañosa, A. González-Comas, E. Obradó, A. Planes, V. A. Chernenko, V. V. Kokorin and E. Cesari: Phys. Rev. B **55** (1997) 11068–11071.
31) V. A. Chernenko, V. A. L'vov, M. Pasquale, C. P. Sasso, S. Besseghini and D. A. Polenur: Int. J. Appl. Electromagn. Mech. **12** (2000) 3–8.